Scripta Materialia 214 (2022) 114681

Contents lists available at ScienceDirect

Scripta Materialia

journal homepage: www.journals.elsevier.com/scripta-materialia

Effect of hybridization in PdAlY-(Ni/Au/Ir) metallic glasses thin films on electrical resistivity

Hanna Bishara [a,*], P. Kontis [a,b], Gerhard Dehm [a], Jochen M. Schneider [c], Simon Evertz [a,c]

[a] Max-Planck-Institut für Eisenforschung, Max-Planck-Str. 1, 40237 Düsseldorf, Germany
[b] Department of Materials Science and Engineering, NTNU Norwegian University of Science and Technology, Trondheim, 7491, Norway
[c] Materials Chemistry, RWTH Aachen University, Kopernikusstr. 10, 52074 Aachen, Germany

ARTICLE INFO

Keywords:
Metallic glass
Thin films
Electrical resistivity
Electronic structure
Hybridization

ABSTRACT

Thin film metallic glasses (MGs) are promising materials for electronic applications. While the transport properties of MGs are composition dependent, the influence of hybridization on the resistivity has not been investigated systematically. We implement a correlative experimental and computational approach utilizing thin film deposition, electrical resistivity measurements, synchrotron X-ray diffraction and *ab initio* calculations to explore the relationship between the fraction of hybridized bonds present in PdAlY-M glasses with *M*=Ir,Au,Ni, where the electrical behavior is dominated by d-electrons. The strong bonds hybridization in PdAlY-Ir yields a high resistivity of 175 μΩm, while the weakly hybridized bonds in PdAlY-M MGs (*M* = Au, Ni) result in lower resistivities of 114 and 92 μΩm, respectively. We propose that an increase in the amount of anti-bonding states close to the Fermi level yields an increased room temperature resistivity.

Thin film metallic glasses (MG) exhibit – in addition to a superior combination of mechanical properties and corrosion resistance [1] – fascinating transport properties. Thus, they enable applications in electronic systems such as the next generation of resistive random-access memory (RRAM), resulting in decreased power consumption and increase the device operation speed [2,3]. In addition, the absence of grain boundaries in the MGs allows for the application as diffusion barrier for metallization layers in integrated circuits [4], solar cells [5], and thermoelectric materials [6]. Moreover, thin film MGs are reported to improve the performance of microelectronic devices such as thin film metal-insulator-metal diodes [7]. The MGs transport properties together with the plasticity enables the application in flexible electronics and skin-attachable devices [8–10]. Pd-based metallic glasses are employed in fast-response capacitive MEMS hydrogen sensors [11], catalytic activity applications [12], hydrogen electro-storage devices [13], and mechanical pressure sensor membrane [14].

Alloying MGs significantly affects their electrical resistivity. For instance, increasing the Al content in Ca-Mg-Al alloys, increases the resistivity due to a change of the Fermi level relatively to the valence band [15]. Another example, alloying Ag-Cu with an increasing amount of Ge causes a gradual increase in resistivity values, which is accompanied with a change of temperature coefficient of resistivity (TCR) from positive to negative values [16]. Alloying Mg-Zn with Ga decreases the density of states at the Fermi level, and consequently increases resistivity [17]. For Pd-Cu-Si thin film MGs, the electrical resistivity can be tuned by controlling their stoichiometry, with resistivity decreasing for increasing Pd on the expense of Si [18]. However, the origin of resistivity-chemistry relationship has not been investigated yet.

Frequent electron scattering due to short-range atomic order affects the unique electrical properties of MGs. Consequently, MGs exhibit a lower electron mean free path and elevated resistivity values compared to crystalline metals. The mechanism for electron conduction can vary between chemically different MGs, and is usually reflected in concomitantly varied absolute resistivity values and TCR. Low resistivity MGs usually follow the nearly-free electron model. However, a high resistivity in MGs is usually attributed to localization of electrons [19], and consequently the nearly-free electron model is no longer valid. Still, there is a dispute on the relationship between the resistivity value and type of conduction electrons, i.e. contributions from the sp-bands or d-band. Some reports claim that high resistivity results from dominating sp-band electrons [20], while others claim that dominating d-band electrons cause the high resistivity [15,21].

The resistivity-temperature dependence in MGs is small compared to the residual resistivity value, i.e. resistivity changes by only few percent

* Corresponding author at: Max-Planck-Institut für Eisenforschung GmbH: Max-Planck-Institut fur Eisenforschung GmbH, Max-Planck-Straße, 1, 40237 Düsseldorf, Germany.
E-mail address: h.bishara@mpie.de (H. Bishara).

https://doi.org/10.1016/j.scriptamat.2022.114681
Received 4 February 2022; Accepted 15 March 2022
Available online 19 March 2022

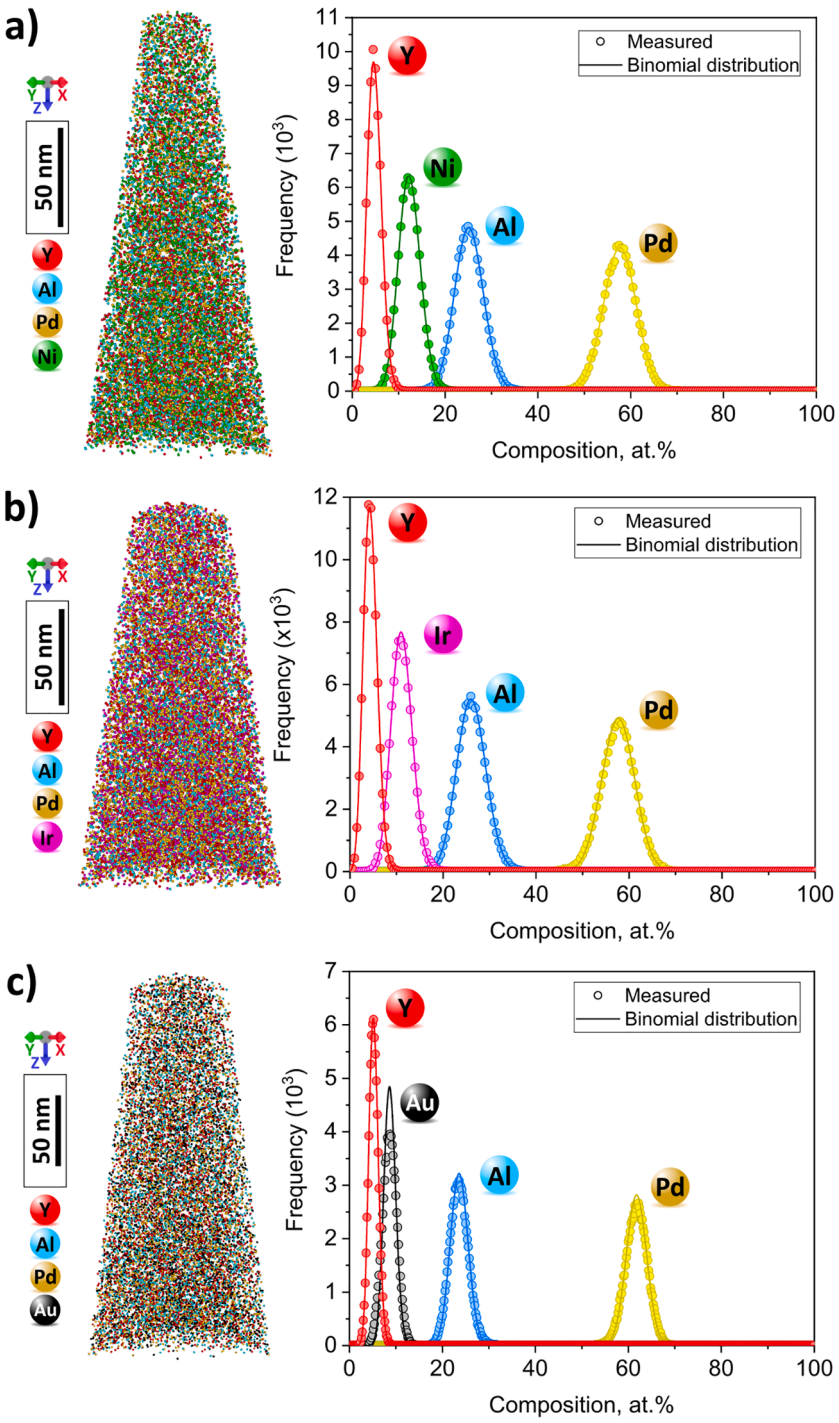

Fig. 1. APT reconstruction and frequency distribution analysis of a) $Pd_{55.9}Al_{26.1}Y_{5.1}Ni_{11.5}$, b) $Pd_{56.7}Al_{27.2}Y_{4.6}Ir_{11.4}$ and c) $Pd_{61.1}Al_{24.7}Y_{5.4}Au_{8.7}$.

within a 100 K range [16]. Increasing the residual resistivity may change the TCR from positive to negative [16]. The universal TCR dependence on residual resistivity is explained based on the Faber-Ziman theory, which confirms the validity of the Boltzmann model of nearly-free electron conductivity, despite possible electron localization. Briefly, the model suggests that additionally to the residual resistivity, the total resistivity of a MG at a finite temperature is caused by electron-electron and an electron-phonon elastic scattering [16]. The former is dominant for the low resistivity regime with positive TCR, while the latter dominates for high resistivity regimes with a negative TCR [16,21,22]. However, it must be noted that the electron transport mechanisms in MG can be affected by alloying: For example, the alloying elements in Mg-based MGs, such as Ga, are decisive for this family of glasses following the nearly-free electron model [17,23].

From the above discussion it is evident that the causality between chemically induced changes in electronic structure of MGs and the associated variations in transport properties are not well understood, which limits knowledge-based materials design efforts of MGs for electronic applications.

In this study, we focus on the PdAlY-M (M= Ir, Au, Ni) system, which exhibits a high fracture toughness as predicted based on the electronic structure and extensive changes in chemical bonding [24]. The fracture toughness has been shown to scale with the amount of localized electron states at the Fermi level, whereby a low amount of localized states

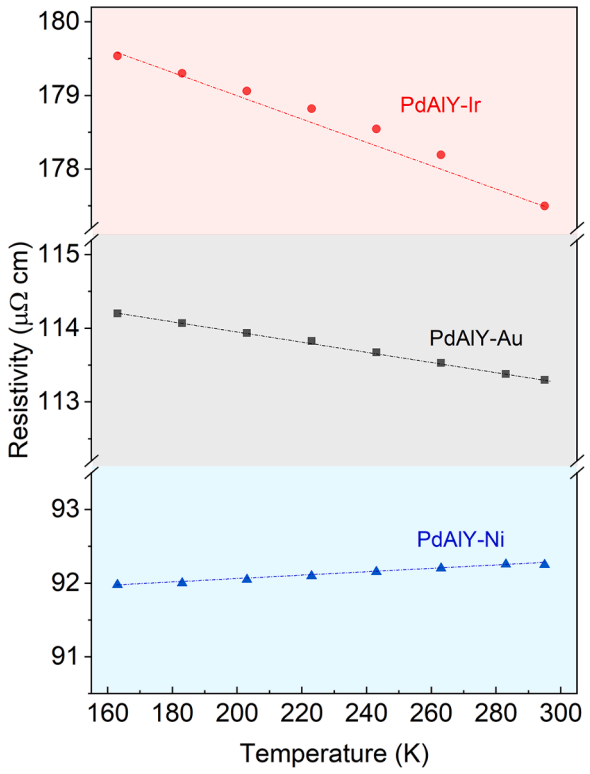

Fig. 2. Temperature dependence of the electrical resistivity of PdAlY-Ir, PdAlY-Au and PdAlY-Ni alloys as a function of temperature. Resistivity of the films is highly dependent on the alloying element. TCR changes from positive to negative values with increasing absolute values of resistivity, following Mooij universal trend. Dotted lines are provided as guide for the eye to show the trend of the TCR.

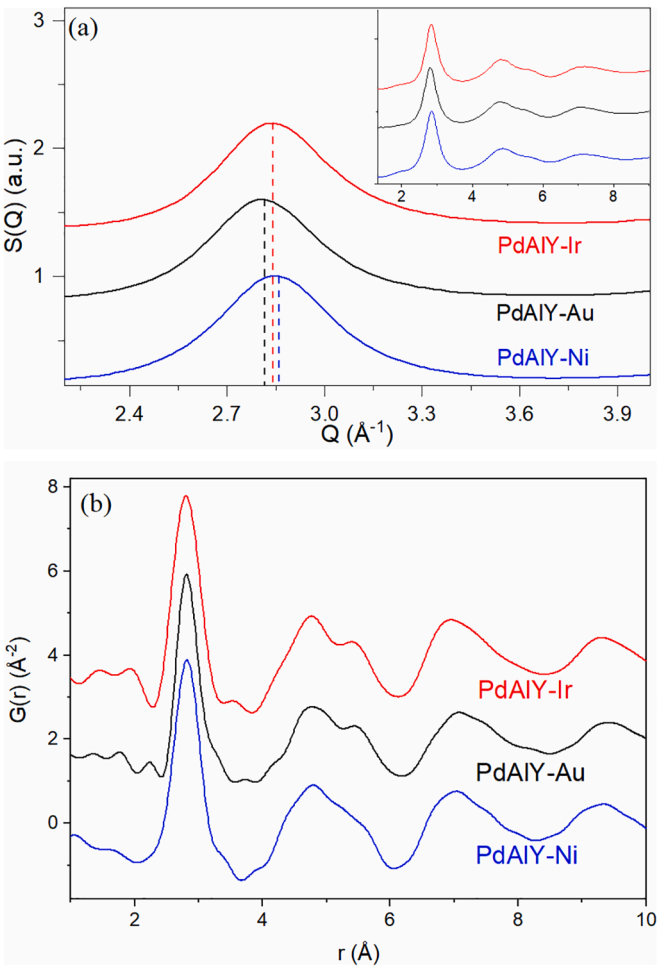

Fig. 3. (a) First peak (and spectrum in inset) of the X-ray Synchrotron normalized diffraction for the three alloys. No pronounced differences are observed in peak position and width between the MG with different alloying elements. (b) Pair distribution functions of the alloys indicating a similar short-range order for all three glasses. Peaks at positions lower than the principal peak at 2.8 Å are caused by the limited q-range available in the diffraction data.

indicates predominantly metallic bonding and yields a high fracture toughness [24]. A systematic study of the M element, where the M element is substituted by Fe, Ni, Co, Cu, Os, Ir, Pt, and Au has identified different fractions of hybridized bonds within the respective PdAlY-M systems [24]. As representative materials for a high and low fraction of hybridized bonds, the PdAlY-Ir, PdAlY-Au and PdAlY-Ni systems have been selected. While the fraction of hybridized bonds in PdAlY-Ir is high, hybridization has been shown to be significantly low in PdAlY-M with *M* = Au, Ni [24]. Hence, we investigate the causality between hybridization in magnetron sputtered PdAlY-based MGs and their electrical resistivity by *ab initio* calculations, high-energy X-ray diffraction and temperature dependent resistivity measurements.

Thin film MGs were synthesised by magnetron sputtering of elemental targets in an ultra-high vacuum combinatorial growth system with a base pressure $<5 \cdot 10^{-7}$ mbar [25]. Ar was used as a working gas with a pressure of $4 \cdot 10^{-3}$ mbar. Silicon was used as substrate for resistivity measurements and polyimide (Kapton®) was utilized for the diffraction experiments, to prevent strong background scattering. The following power densities were applied to the targets: 4.3 W/cm^2 for Pd, 4.7 W/cm^2 for Al, 1.8 W/cm^2 for Y, 2.5 W/cm^2 for Ir, 0.9 W/cm^2 for Au, and 1.4 W/cm^2 for Ni. The target to substrate distance was 10 cm and the sample was not rotated during synthesis to obtain Pd-Al and Y-M gradients, from which the position with the composition closest to the calculated composition was chosen.

Morphology and microstructure of the films were inspected with a scanning electron microscopy (SEM) (Auriga, Zeiss) top-view and cross-section imaging. Atom probe tomography (APT) specimens were prepared from the center of the metallic glass thin film deposited on a silicon substrate using an FEI Helios 600 following the procedures described in Ref [26].. APT measurements were carried out on a Cameca LEAP 3000 HR operated in voltage mode at a pulse repetition rate ranging between 100 and 200 kHz, a pulse rate of 15% and the base temperature was set to 60 K. Data analysis was performed using the IVAS 3.8.2 software package. Thicknesses of the films were obtained by measuring the edge-profile of the film with a Keyence VK-4000 laser microscope.

The electrical resistivity measurements of the thin films were carried out by adapting the Van der Pauw method [27] in the temperature range between −110 °C and 10 °C. The films were held in a LINKAM - HFS600 probing system, which supplies 4 contacts through 4 tungsten needles supported by springs. Controlling temperature of the sample was obtained by a liquid nitrogen pump and a suitable controller (LINKAM - LNP) connected to the stage of the probing system. The temperature was measured by thermocouples within the stage. Cooling started from 20 °C with a rate of 5 °C/min. The temperature was decreased in steps of 20 °C and kept constant for 6 min at each step. The resistivity measurements were conducted 4 mins after reaching the desired temperature, which is a sufficient time for thermal equilibrium. The temperature profile is shown in Fig. S1, the red markers indicate the electrical measurement time, and the inset illustrates the resistivity experimental setup. A function generator (Keithly 6221) supplied 100 DC pulses of 50 mA with a pulse with of $5 \cdot 10^{-3}$ s, while the voltage was measured at the pulse half-time through a nanovoltmeter (Keithly 2182A). The deadtime between subsequent pulses is set to 20 times the pulse time duration to avoid electrical field overlapping. The pulsed measurements were

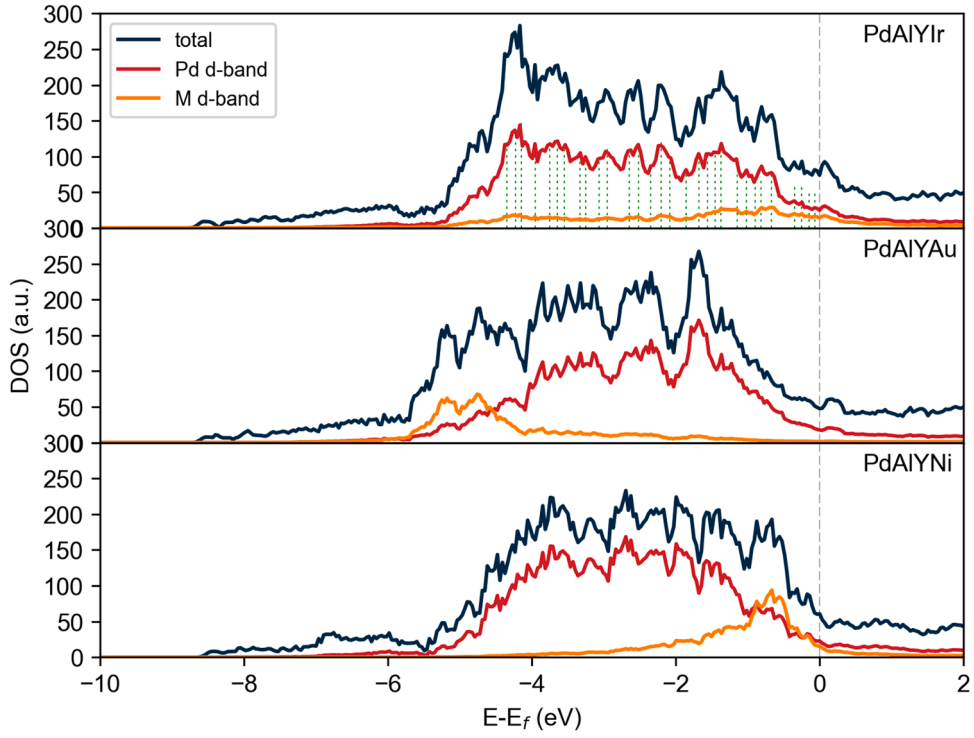

Fig. 4. Total density of states as well as d-band of Pd and M for PdAlY-M with M = Ni, Au, Ir. Strong hybridization of the Pd and Ir d-bands is observed and marked with green dashed lines.

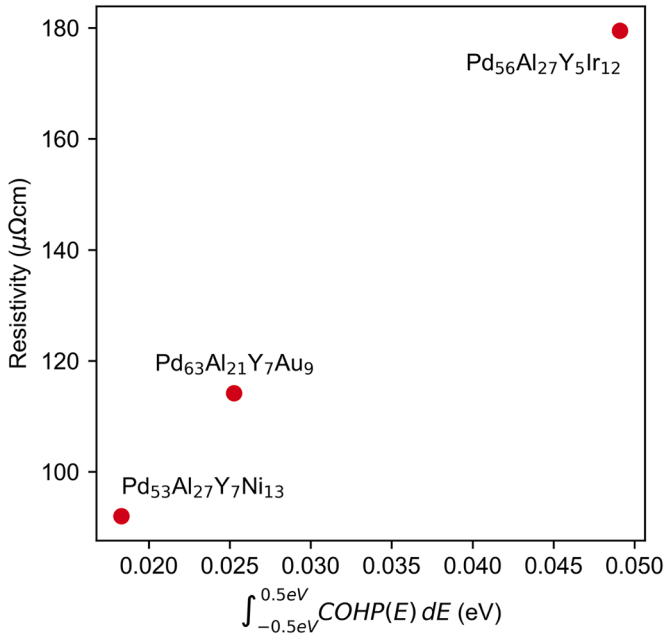

Fig. 5. Electrical resistivity as a function of integrated COHP around the Fermi level.

performed to ensure thermal stability which is confirmed by similar repeated electrical measurements [28]. The resistivity is averaged over 100 measurements per temperature.

High-energy X-ray diffraction (HEXRD) on the samples synthesised on polyimide was performed at beamline P02.1 of the electron-storage ring PETRAIII at DESY [29], Hamburg. The X-rays had a wavelength of 20.701 pm and were detected with a Perkin Elmer XRD1621 fast detector. The data was integrated employing the FIT2D software [30, 31]. To obtain the real-space pair distribution function (PDF), the diffractograms were corrected for background scattering and the PDF calculated by a fast Fourier transform implemented in the PDFgetX3 software [32].

Density-functional theory based *ab initio* calculations were conducted in [16] to determine the electronic structure [33]. Therefore, iterative heating-quenching cycles according to Hostert et al [34]. were performed on supercells containing 115 atoms and employing the openMX [35–37] and the Vienna Ab Initio Simulation Package (VASP) [38,39]. Details of the calculations are given in [24].

Three alloy thin films were deposited on Si substrates. No significant differences in the film's morphology observed are by SEM (Fig. S2). APT revealed the composition of the films to be $Pd_{56.7}Al_{27.2}Y_{4.6}Ir_{11.4}$, $Pd_{61.1}Al_{24.7}Y_{5.4}Au_{8.7}$, and $Pd_{55.9}Al_{26.1}Y_{5.1}Ni_{11.5}$, with thicknesses of 6.4, 1 and 1 μm, respectively. The APT reconstructions of the three glasses in Fig. 1 indicate no obvious clustering of elements. The frequency distribution analysis confirms that the distribution of each of the species is comparable to a binomial distribution and hence suggests a homogeneous distributions of the elements within the resolution limits of APT [40,41].

The electrical resistivity and its temperature-dependence (TCR) are presented in Fig. 2. Thickness variations of the film can be excluded to influence the resistivity of the film, as the films with thicknesses of >1 μm exceed the electron mean free path, which is on the order of nm, by orders of magnitude. Both are depending on the alloying element. PdAlY-Ni films exhibit the lowest resistivity and a positive TCR, with a linear relationship between resistivity and temperature. The PdAlY-Au alloy has 23% larger resistivity value, and the resistivity-temperature relation maintains linearity but with a negative TCR value. The PdAlY-Ir thin film shows the highest resistivity among the films, with a negative TCR, and non-linear resistivity-temperature relation. The trend that TCR changes from positive to negative values with increasing the residual resistivity values is consistent with Mooij universal trend [16, 42]. Here TCR = 0 occurs at around 100 μΩ•cm. The resistivity-temperature relationship is determined by a complex interplay of the electron-phonon scattering and electron-electron scattering.

While the first mechanism dominates at low residual resistivity values and causes a resistivity increase with temperature, the latter is dominant at high residual resistivity values and yields a resistivity decrease with temperature [16]. The non-metallic temperature behavior for high resistivity glasses such as PdAlY-Ir and PdAlY-Au in this study indicates weak localization according to Howson [19], which is consistent with the electron-electron scattering notion by Mooij [16,39].

In the following, topology and electronic structure are analysed in an effort to identify the origin of the different electrical resistivity values.

The topology of the thin film MGs is investigated by the normalized structure factor S(Q), shown in Fig. 3a. The position of the principle peak of the S(Q) is an indicator for the mean atomic distance as well as the position of the Fermi level according to the free electron model of Nagel and Tauc [43]. For the PdAlY-M glasses, the principle peak (Fig. 3a) is similar for the three Pd-based metallic glasses with positions of 2.851 $Å^{-1}$ for PdAlY-Ni, 2.814 $Å^{-1}$ for PdAlY-Au and 2.848 $Å^{-1}$ for PdAlY-Ir. Also, the second and third peak of S(Q) resemble each other, as shown in the Fig. 3a inset. Hence, the mean atomic volume in all three PdAlY-M glasses is comparable. An additional parameter that describes the short-range atomic order is the pair distribution function G(r), where r is the distance between atoms. Analysis of G(r), presented in Fig. 3b, indicates a similar short-range order for the three glasses. While peak positions are not equal due to differences in atomic radii of the M element, the shape of G(r) and thus the motifs of the short-range order resemble each other. Therefore, the differences of the residual resistivity do not seem to originate in the short-range order [44]. Hence, the electronic structure is considered.

The analysis of the electronic structure based on the density of states (Fig. 4). The energy of the electronic states is normalized to the Fermi level, which corresponds to the highest occupied Kohn-Sham state of the *ab initio* calculations. As the partial DOS of the s- and p-bands of the Pd and M element are small compared to the partial DOS of the d-bands and the contribution of the other elements to the overall bonding does not change significantly [24], the DOS analysis focuses on the electrons in the d-bands of Pd and M, which dominate the total density of states (DOS). Hence, the d-band electrons dominate the electrical conductivity of the Pd-based glass alloys, regardless of the resistivity magnitude. This observation is consistent with reports for various transition metal based MGs [45–47], while the s- and p-electrons gain importance with an increasing amount of main group elements [15,20].

As indicated by the non-metallic temperature behavior and its origin in electron-electron scattering [19], an important factor in the electron transport properties of MGs is the hybridization and hence localization of electrons. In fact, the DOS show an overlap of peak positions and shapes between the d-bands of Pd and Ir (Fig. 4). Hence, PdAlY-Ir exhibits hybridization between Pd and Ir d-bands. Significantly less hybridization is observed in Fig. 4 between the d-bands of Pd and Au/Ni, [24], where the Ni/Au d-band occupies only a narrow energy range which is not dominated by the Pd d-band. However, this narrow energy range populated by the d-electrons is close to the Fermi level for PdAlY-Ni, while it is in the energy range of −6 to −4 eV for PdAlY-Au. Therefore, hybridization is strongest in the PdAlY-Ir MG and lowest in the PdAlY-Ni MG [24]. This is consistent with electron localization [19] and the temperature coefficient of resistivity in Fig. 2.

To further inspect the electronic structure differences between the alloys, the crystal orbital Hamilton population (COHP) is inspected, i.e. weighting the DOS by band structure energy [48]. The COHP analysis is done in Fig. 2a of reference [24]. A positive COHP indicates an anti-bonding contribution to the overall bonding, whereas negative COHP imply bonding contributions [49]. The DFT calculations yield positive COHP values for all glasses close to the Fermi level, hence, all three glasses exhibit anti-bonding states ([24], Fid. 2a). Integrating over the contributions in the vicinity of Fermi level between −0.5 and 0.5 eV, which are relevant for electrical resistivity, shows that the resistivity scales with an increasing amount of anti-bonding states around the Fermi level (Fig. 5). Similar results are obtained for different integration intervals. In the light of the similar short-range order and the scaling of the resistivity with anti-bonding states around the Fermi level, we induce that the electrons in metallic glasses cannot be treated as "nearly-free" as in the Faber-Ziman theory [44]. Instead, the room temperature resistivity is dominated by the electron-electron interactions.

In conclusion, the amount of anti-bonding states as determined by the COHP close to the Fermi level determines the room temperature electrical resistivity of the PdAlY-based thin film MGs. The electrical resistivity has been shown to scale with integrated COHP in the surroundings of the Fermi level, indicating that the electron-electron interaction are the origin of the resistivity, since the topology of the three PdAlY-(Ir, Au, Ni) MG is similar. To understand the temperature coefficient of resistivity in the future, changes of the anti-bonding states close to the Fermi level with temperature need to be understood, which is cannot be probed with available ground-state DFT methods.

Declaration of Competing Interest

The authors declare that they have no known competing financial interests or personal relationships that could have appeared to influence the work reported in this paper.

Acknowledgments

Authors thank Daniel Gall for the fruitful discussion. Baptiste Gault, Uwe Tezins and Andreas Sturm are acknowledged for their support to the FIB & APT facilities at MPIE. Authors thank Ines Kirchlechner for the experimental support. H.B and G.D. acknowledge the financial support by the ERC Advanced Grant GB CORRELATE (Grant Agreement 787446 GB-CORRELATE) and the German Science Foundation within the SPP1594 "Topological Engineering of Ultrastrong Glasses" (Grant Nr. DE 796/9–2). We acknowledge DESY (Hamburg, Germany), a member of the Helmholtz Association HGF, for the provision of experimental facilities. Parts of this research were carried out at beamline P02.1 of PETRA III. Beamtime was allocated for proposal I-20160587. Computational resources were provided by the Jülich-Aachen Research Alliance (JARA) on the HPC cluster CLAIX of RWTH Aachen University under the projects JARA0131.

Supplementary materials

Supplementary material associated with this article can be found, in the online version, at doi:10.1016/j.scriptamat.2022.114681.

References

[1] P. Yiu, W. Diyatmika, N. Bönninghoff, Y.-.C. Lu, B.-.Z. Lai, J.P. Chu, J. Appl. Phys. 127 (2020) 30901.
[2] B. Tulu, J.P. Chu, S.-.F. Wang, Mater. Chem. Phys. 168 (2015) 95–100.
[3] W. Diyatmika, T.-.Y. Wang, J.P. Chu, S.-.F. Wang, Thin Solid Films 688 (2019), 137450.
[4] C.-.W. Wang, P. Yiu, J.P. Chu, C.-.H. Shek, C.-.H. Hsueh, J. Mater. Sci. 50 (2015) 2085–2092.
[5] W. Diyatmika, L. Xue, T.-.N. Lin, C. Chang, J.P. Chu, Jpn. J. Appl. Phys. 55 (2016) 80303.
[6] C.-.C. Yu, H. Wu, M.T. Agne, I.T. Witting, P.-.Y. Deng, G.J. Snyder, J.P. Chu, APL Mater. 7 (2019) 13001.
[7] N. Alimardani, J.F. Conley, Appl. Phys. Lett. 105 (2014) 82902.
[8] C. Qin, D. Zheng, Q. Hu, X. Zhang, Z. Wang, Y. Li, J. Zhu, J.Z. Ou, C. Yang, Y. Wang, Appl. Mater. Today 19 (2020), 100539.
[9] H.J. Xian, C.R. Cao, J.A. Shi, X.S. Zhu, Y.C. Hu, Y.F. Huang, S. Meng, L. Gu, Y. H. Liu, H.Y. Bai, W.H. Wang, Appl. Phys. Lett. 111 (2017), 121906.
[10] S. Lee, S.-.W. Kim, M. Ghidelli, H.S. An, J. Jang, A.L. Bassi, S.-.Y. Lee, J.-.U. Park, Nano Lett. 20 (2020) 4872–4881.
[11] H. Yamazaki, Y. Hayashi, K. Masunishi, D. Ono, T. Ikehashi, Electron. Commun. Jpn. 102 (2019) 70–77.
[12] B. Sarac, T. Karazehir, Y.P. Ivanov, B. Putz, A.L. Greer, A.S. Sarac, J. Eckert, Nanoscale 12 (2020) 22586–22595.
[13] B. Sarac, T. Karazehir, M. Mühlbacher, B. Kaynak, C. Gammer, T. Schöberl, A. S. Sarac, J. Eckert, ACS Appl. Energy Mater. 1 (2018) 2630–2646.
[14] N. Van Toan, T.T.K. Tuoi, Y.-.C. Tsai, Y.-.C. Lin, T. Ono, Sci. Rep. 10 (2020) 10108.

[15] U. Mizutani, M. Sasaura, Y. Yamada, T. Matsuda, J. Phys. F Met. Phys. 17 (1987) 667–678.
[16] U. Mizutani, K. Sato, I. Sakamoto, K. Yonemitsu, J. Phys. F Met. Phys. 18 (1988) 1995–2007.
[17] T. Matsuda, N. Shiotani, U. Mizutani, J. Phys. F Met. Phys. 14 (1984) 1193–1204.
[18] R. Yamauchi, S. Hata, J. Sakurai, A. Shimokohbe, Jpn. J. Appl. Phys. 45 (2006) 5911–5919.
[19] M.A. Howson, J. Phys. F Met. Phys. 14 (1984) L25–L31.
[20] N.F. Mott, Philos. Mag. A J. Theor. Exp. Appl. Phys. 19 (1969) 835–852.
[21] J. Antonowicz, A. Pietnoczka, K. Pękała, J. Latuch, G.A. Evangelakis, J. Appl. Phys. 115 (2014), 203714.
[22] U. Mizutani, Prog. Mater. Sci. 28 (1983) 97–228.
[23] U. Mizutani, T. Matsuda, J. Phys. F Met. Phys. 14 (1984) 2995–3006.
[24] S. Evertz, I. Kirchlechner, R. Soler, C. Kirchlechner, P. Kontis, J. Bednarcik, B. Gault, G. Dehm, D. Raabe, J.M. Schneider, Mater. Des. 186 (2020), 108327.
[25] V. Schnabel, M. Köhler, S. Evertz, J. Gamcova, J. Bednarcik, D. Music, D. Raabe, J. M. Schneider, Acta Mater. 107 (2016) 213–219.
[26] K. Thompson, D. Lawrence, D.J. Larson, J.D. Olson, T.F. Kelly, B. Gorman, Ultramicroscopy 107 (2007) 131–139.
[27] I. Miccoli, F. Edler, H. Pfnür, C. Tegenkamp, J. Phys. Condens. Matter 27 (2015), 223201.
[28] H. Bishara, M. Ghidelli, G. Dehm, ACS Appl. Electron. Mater. 2 (2020) 2049–2056.
[29] A.-.C. Dippel, H.-.P. Liermann, J.T. Delitz, P. Walter, H. Schulte-Schrepping, O. H. Seeck, H. Franz, J. Synchrotron Radiat. 22 (2015) 675–687.
[30] A.P. Hammersley, S.O. Svensson, A. Thompson, Nucl. Instruments Methods Phys. Res. Sect. A Accel. Spectrometers, Detect. Assoc. Equip. 346 (1994) 312–321.
[31] A.P. Hammersley, S.O. Svensson, M. Hanfland, A.N. Fitch, D. Hausermann, High Press. Res. 14 (1996) 235–248.
[32] P. Juhás, T. Davis, C.L. Farrow, S.J.L. Billinge, J. Appl. Crystallogr. 46 (2013) 560–566.
[33] P. Hohenberg, W. Kohn, Phys. Rev. 136 (1964) B864–B871.
[34] C. Hostert, D. Music, J. Bednarcik, J. Keckes, V. Kapaklis, B. Hjörvarsson, J. M. Schneider, J. Phys. Condens. Matter 23 (2011), 475401.
[35] T. Ozaki, Phys. Rev. B 67 (2003), 155108.
[36] T. Ozaki, H. Kino, Phys. Rev. B 69 (2004), 195113.
[37] T. Ozaki, H. Kino, Phys. Rev. B 72 (2005) 45121.
[38] G. Kresse, J. Furthmüller, Phys. Rev. B 54 (1996) 11169–11186.
[39] G. Kresse, D. Joubert, Phys. Rev. B 59 (1999) 1758–1775.
[40] B. Gault, B. Klaes, F.F. Morgado, C. Freysoldt, Y. Li, F. De Geuser, L.T. Stephenson, F. Vurpillot, Microsc. Microanal. (2021) 1–11.
[41] F. De Geuser, B. Gault, Acta Mater. 188 (2020) 406–415.
[42] J.H. Mooij, Phys. Status Solidi 17 (1973) 521–530.
[43] S.R. Nagel, J. Tauc, Phys. Rev. Lett. 35 (1975) 380–383.
[44] J.M. Ziman, Philos. Mag. A J. Theor. Exp. Appl. Phys. 6 (1961) 1013–1034.
[45] R. Schulz, M. Mehra, W.L. Johnson, J. Phys. F Met. Phys. 15 (1985) 2109–2120.
[46] D. Pavuna, J. Non. Cryst. Solids 61–62 (1984) 1353–1358.
[47] U. Mizutani, M. Tanaka, H. Sato, J. Phys. F Met. Phys. 17 (1987) 131–141.
[48] V.L. Deringer, A.L. Tchougréeff, R. Dronskowski, J. Phys. Chem. A 115 (2011) 5461–5466.
[49] R. Dronskowski, P.E. Bloechl, J. Phys. Chem. 97 (1993) 8617–8624.